

---

# LOFAR as a Lightning Mapping Array

---



*Author:*  
Danny SARDJAN

*Supervisors:*  
prof. dr. Olaf SCHOLTEN  
prof. dr. Mariano MENDEZ  
dr. Qader DOROSTI HASANKIADEH



UNIVERSITY OF GRONINGEN

BACHELOR OF SCIENCE ASTRONOMY

KVI - CENTER FOR ADVANCED RADIATION TECHNOLOGY

KAPTEYN INSTITUTE

---

# LOFAR as a Lightning Mapping Array

---

*Author:*  
Danny SARDJAN

*Supervisors:*  
prof. dr. Olaf SCHOLTEN  
prof. dr. Mariano MENDEZ  
dr. Qader DOROSTI HASANKIADEH

July 18, 2016

## Abstract

In order for the lightning process to occur it turns out that a number of conditions have to be met. A thunderstorm with a sufficiently strong electric field, icy particles and free electrons. In order to acquire the free electrons it turns out that extensive air showers from cosmic rays are crucial. It is shown that these cosmic rays originate from sources such as supernova remnants and active galactic nuclei. After lightning inception a stepped leader is formed. This leader will form a conducting channel between the cloud and the ground. When this leader reaches the ground a return stroke will take place and neutralize the channel. When a stepped leader is formed a pulse is emitted and it turns out that the low band antennas of LOFAR can measure this signal. To find the location of the stepped leader in space and time it is crucial to synchronize these signals in time and this has been done successfully. Furthermore the difference in pulse shape tells us something about the direction of the stepped leader.



## Acknowledgments

First and foremost I would like to thank Prof. Olaf Scholten for giving me the opportunity to do lightning research and for his guidance and enthusiasm surrounding the project. He has given me a good look into doing research and I got a feel for the scientific community through meetings and the ARENA conference in Groningen.

Furthermore I would like to thank Dr. Qader Dorosti Hasankiadeh for the collaboration on the data analysis and for the insightful remarks on my thesis.

I would also like to thank Gia Trinh and Jeroen Muller for helping me with understanding the python program we used for analyzing the data.

Finally, I would like to thank my fellow bachelor students with whom I spent a lot of time in the computer cluster at the KVI. There was a good atmosphere and during the breaks we could always discuss problems we had regarding our research.

# Contents

<b>1</b>	<b>Introduction</b>	<b>4</b>
<b>2</b>	<b>Lightning</b>	<b>5</b>
2.1	Lightning Inception . . . . .	5
2.2	Lightning Discharges . . . . .	5
<b>3</b>	<b>Cosmic Rays</b>	<b>7</b>
3.1	Acceleration Mechanism . . . . .	8
3.2	Sources of Cosmic Rays . . . . .	11
3.2.1	Supernova Remnants . . . . .	12
3.2.2	Galactic Centre . . . . .	13
3.2.3	Active Galactic Nuclei . . . . .	14
<b>4</b>	<b>Lightning Mapping Array</b>	<b>16</b>
4.1	Accuracy of the Lightning Mapping Array in New Mexico . . . . .	16
4.2	LOFAR as a Lightning Mapping Array . . . . .	17
<b>5</b>	<b>Lightning Observations</b>	<b>19</b>
5.1	Lightning observations with LOFAR . . . . .	19
5.2	Data analysis . . . . .	19
5.2.1	Time trace measurement . . . . .	19
5.2.2	Time synchronization . . . . .	20
5.2.3	Pulse shape . . . . .	22
5.2.4	Time of arrival method . . . . .	23
<b>6</b>	<b>Conclusion and Outlook</b>	<b>26</b>
<b>7</b>	<b>Appendix</b>	<b>28</b>

# 1 Introduction

Lightning is not a very well-understood process, in particular the stepped leaders which carry the discharge from the clouds are subject to investigation. In my thesis we will start by taking a look at lightning inception. This is a not very well-understood process. It is thought that ice particles in clouds are the starting point for a lightning discharge to take place. It also turns out that free electrons are needed in the vicinity of these ice particles. In order to have access to enough free electrons it is thought that we need extensive air showers from cosmic rays to start the lightning discharge [1]. In section 3 we will look into how cosmic rays get their high energies and what their sources are. Since cosmic rays are charged particles they will be deflected by magnetic fields and we cannot easily trace them back to their source. In section 4 we will investigate how lightning mapping arrays work and how we can use LOFAR as lightning mapping array. Lastly we will work with lightning observations from LOFAR. A major part in finding the origin of the stepped leaders (in space and time) is to know the time differences at which the received pulses arrive at each station. We will synchronize the pulses in time and take a look at the pulse shape as we observe them. Finally some remarks will be made on how to improve our analysis and what needs to be done in order to make LOFAR a lightning mapping array.

## 2 Lightning

### 2.1 Lightning Inception

In order to understand lightning inception a few conditions have been investigated which are necessary for lightning inception [1]. It is thought that this process happens at large ice particles since they will enhance the electric field due to their high electric permittivity ( $\epsilon = 90$ ), so-called hydrometeors. The properties of these hydrometeors are studied at an altitude of 5.5 km. In order to enhance the electric field, the hydrometeors have to line up parallel to the thundercloud such that a charge difference is induced between both ends of the hydrometeor. The shape (expressed in curvature over length) can be plotted against the electric field of the thundercloud. It is concluded that for lightning inception to occur large hydrometeors or a high electric field are necessary.

To obtain pertinent results a specific hydrometeor is taken which has a radius of curvature at the tip of  $R = 0.4$  mm and a length of 6 cm. The hydrometeor typically has a density of  $0.1 \text{ m}^{-3}$  in thunderclouds. Furthermore an electric field of 2.7 kV/cm is assumed in the clouds. In order to start the discharge it is estimated that about 100 free electrons per  $\text{cm}^3$  are necessary. Using these initial conditions, a simulation has been performed. As a result a streamer is formed at the tip of such a hydrometeor. The average velocity of the streamer is  $10^5$  m/s, electron densities reach about  $10^{12}$  electrons per  $\text{cm}^3$  when the simulation runs for 46 nanoseconds. Furthermore it is investigated how often the electron density of  $100 \text{ cm}^{-3}$  is reached at 5.5 km. The sources of these electrons are extensive air showers caused by cosmic rays. The cosmic rays that are studied are protons with energies between  $5 \cdot 10^{15}$  and  $5 \cdot 10^{16}$  eV. For these protons 297 simulations have been performed with software called Corsika. The obtained result suggests that 100 electrons per  $\text{cm}^3$  are reached with a frequency of at least  $5 \text{ km}^{-2} \text{ min}^{-1}$  [1].

For lightning inception to occur, these events need to occur simultaneously in space and time. In addition a thunderstorm electric field is needed, as well as a hydrometeor with the right shape and size and an extensive air shower which creates enough free electrons around our hydrometeor. Given a thundercloud, if the radius of the core of the shower at this altitude is 100 cm and the hydrometeor density is  $10^{-7} \text{ cm}^{-3}$  then a height of 3 m of the shower core is sufficient. Furthermore, the electric field within this volume has to exceed  $2.7 \text{ kV/cm}^{-1}$  [1].

### 2.2 Lightning Discharges

Following lightning inception a process called lightning discharge will occur. We will look at negative lightning discharges to the ground. This discharge from a cloud to the ground is also called a return stroke. In order for this discharge to take place, we need a sufficient charge separation in a cloud. Thunderclouds have a positive charge density at the upper part of the cloud, a negative charge in the lower part of the cloud, and just below this there is another positively charged area (which has a smaller positive charge than the upper part of the cloud). After lightning inception a process called the preliminary breakdown will take place in the cloud. Following this process a stepped leader is formed, which leads the lightning discharge towards the ground and propagates through the sky in steps. These steps are typically  $1 \mu\text{s}$  in duration, bridging a distance of tens of meters with a time interval between steps of 20 to  $50 \mu\text{s}$  [2]. Out of these stepped leaders a conducting path is formed between the cloud and the ground. The electric potential difference between a stepped leader and the ground is thought to be in the order of tens of megavolts. The limits of this potential difference can be estimated by multiplying the typical observed electric field in the cloud ( $10^5 \text{ V m}^{-1}$ ) and the

expected electric field at the ground underneath a thundercloud right before the lightning discharge ( $10^4 \text{ V m}^{-1}$ ) with the minimum height of the cloud ( $\sim 5 \text{ km}$ ). This calculation gives us a range of 50 to 500 MV. In 2001 measurements of the electric field of the thunderstorms were done with sounding balloons, where the measurements show that the maximum value of the potential of a cloud would be from -102 to +94 MV.

When the stepped leader approaches the ground the electric field above the ground increases until a critical value is reached which initiates one or more upward connecting leaders. Some tens of meters above the ground the stepped leader attaches itself to the upward connecting leader. Immediately after this process a return stroke will initiate and this neutralizes the leader charge. This return stroke typically has a speed between one-third and one-half of the speed of light [2]. Furthermore this return stroke current has an initial peak of about 30 kA and then decays quickly (in the order of microseconds). The lighting channel will be heated up because of this return stroke and will reach a temperature of about 30 000 K, as a result of which the channel pressure will become 10 atm or more. This will expand the channel, causing optical radiation and a shock wave which becomes the thunder we can hear. After this first return stroke subsequent strokes occur between the cloud and the ground.

### 3 Cosmic Rays

Cosmic rays are charged particles with very high energies. These particles collide with the atmosphere of Earth causing extensive air showers. As we will see in this chapter, they originate from galactic and extragalactic sources. Cosmic rays have been heavily studied for their origin and composition. Since cosmic rays are charged, they will be deflected by magnetic fields. Therefore we cannot simply trace a cosmic ray back to its source. Around 85% of cosmic rays are protons, alpha particles make up 12 % of cosmic rays and the other cosmic rays consist of heavier elements, electrons and photons [3].

In figure 1 we see the spectrum of the cosmic rays, the energies are multiplied with  $E^{2.5}$  in order to reveal more features. This spectrum can approximately be described by a power law of the form.

$$\frac{dN}{dE} \sim E^{-\gamma} . \quad (1)$$

With  $\gamma$  of around 2.7. In the spectrum we can observe a couple of features, first there is the knee around an energy of  $3 \cdot 10^{15}$  eV. At this point the spectral index increases to  $\gamma \simeq 3$ . At these energies the galactic magnetic field cannot contain the cosmic rays anymore and they diffuse out of the galaxy. Then there is the ankle around an energy of  $3 \cdot 10^{18}$  eV. This is thought to be a transition area between galactic and extragalactic sources of cosmic rays [3]. Finally there is the GZK (Greisen-Zatsepin-Kuzmin) region, which is a theoretical upper limit for cosmic ray energies. At this point cosmic rays start interacting with the Cosmic Microwave Background (CMB) and lose energy. Since the mean free path of cosmic rays is of the order of 50 Mpc we know that the cosmic rays we observe in this region are most likely from sources within  $\sim 50$  Mpc.

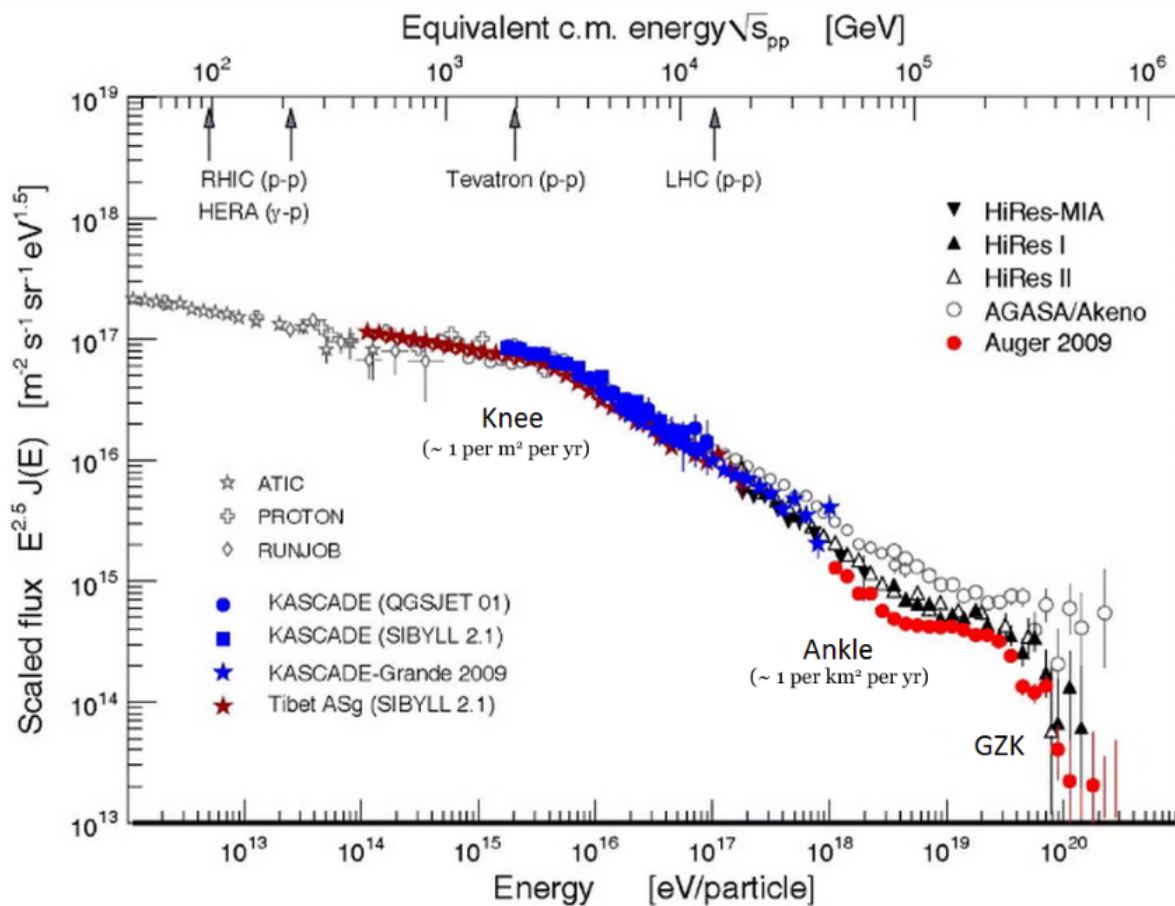


Figure 1: The cosmic ray spectrum [3]

### 3.1 Acceleration Mechanism

As early as 1949, it was suggested by Fermi [4] that cosmic rays could originate from the interaction of charged particles with magnetic fields in interstellar space. Before this it was suggested that all cosmic rays would originate from the sun. According to the theory of Fermi acceleration the energy of the cosmic ray steadily increases when it collides with these magnetic fields, most likely to be found in interstellar clouds of gas.

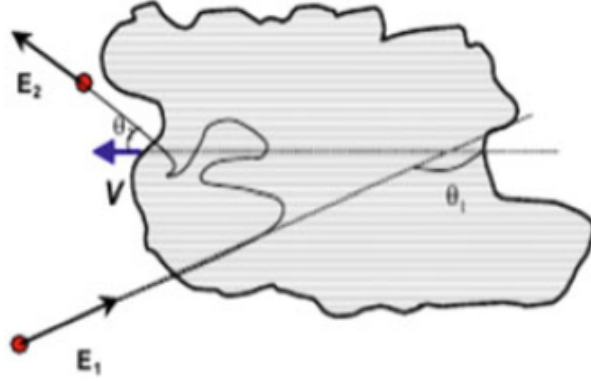


Figure 2: Cosmic ray scattering in a cloud [5]

To derive the energy increase of a particle that collides with magnetic clouds. We consider a cloud moving with a velocity  $\beta = V/c$  and the angles  $\theta_1$  and  $\theta_2$  between the initial and final particle momentum and the velocity of the cloud, as seen in figure 2. In the laboratory frame the particle has an energy  $E_1$ , furthermore the gamma factor is given by  $\gamma = \frac{1}{\sqrt{1-v^2/c^2}}$ , where  $v$  is the velocity of the cloud and  $c$  is the speed of light. In the cloud reference frame the particle has an energy given by:

$$E_1^* = \gamma E_1 (1 - \beta \cos \theta_1) . \quad (2)$$

Note that in the cloud reference frame  $E_1^* = E_2^*$ , so in the laboratory frame the energy after the collision becomes:

$$E_2 = \gamma E_2^* (1 + \beta \cos \theta_2) . \quad (3)$$

So the energy difference becomes:

$$\frac{\Delta E}{E} = \frac{1 - \beta \cos \theta_1 + \beta \cos \theta_2 - \beta^2 \cos \theta_1 \cos \theta_2}{1 - \beta^2} - 1 . \quad (4)$$

Since the particle undergoes a lot of collisions inside the cloud it doesn't matter at what angle the particle came into the cloud. This gives:

$$\langle \cos \theta_2 \rangle = 0 . \quad (5)$$

$$\left\langle \frac{\Delta E}{E} \right\rangle = \frac{1 - \beta \langle \cos \theta_1 \rangle}{1 - \beta^2} - 1 . \quad (6)$$

Now we have to calculate  $\langle \cos \theta_1 \rangle$ . The probability of collision is not constant as a function of  $\theta_1$  since it is more probable that a particle hits the cloud head on than from behind. So the property is dependent on the relative velocities.

$$P \propto (v - V \cos \theta_1) \simeq (1 - \beta \cos \theta_1) . \quad (7)$$

So we get:

$$\langle \cos \theta_1 \rangle = \frac{\int_{-1}^1 \cos \theta_1 (1 - \beta \cos \theta_1) d \cos \theta_1}{\int_{-1}^1 (1 - \beta \cos \theta_1) d \cos \theta_1} = -\frac{\beta}{3} . \quad (8)$$

So the average energy increase becomes:

$$\left\langle \frac{\Delta E}{E} \right\rangle \simeq \frac{4}{3} \beta^2 . \quad (9)$$

Since this energy increase is quadratic in  $\beta$  it is called second-order Fermi acceleration. But since  $\beta$  is usually small ( $\simeq 10^{-4}$ ) this does not explain the energy spectrum of cosmic rays we observe [5].

Later it was suggested that undergoing diffuse shock acceleration would turn the energy gain to be linear in  $\beta$  and this is called first-order Fermi acceleration. The difference with the first situation is that it is assumed that the shock wave is a plane wave. This is a good assumption for supernova remnants, since locally the wave front can be seen as a plane wave. In the frame of the wavefront the medium ahead of the front runs into the front with velocity  $\vec{u}_1$  while the shocked gas behind the wavefront moves away with velocity  $\vec{u}_2$ . In the laboratory frame a particle will collide with the shock front which has a velocity  $V = \vec{u}_1 - \vec{u}_2$ . Since the particle can undergo multiple collisions in this medium around the shock front it can cross the shock front multiple times. In this situation, the angles  $\theta_1$  and  $\theta_2$  have the following constraints:

$$-1 \leq \cos \theta_1 \leq 0 . \quad (10)$$

$$0 \leq \cos \theta_2 \leq 1 . \quad (11)$$

Now the probability of crossing the shock front is proportional to  $\cos \theta$  with the mean values:

$$\langle \cos \theta_1 \rangle = \frac{\int_{-1}^0 \cos^2 \theta_1 d \cos \theta_1}{\int_{-1}^0 \cos \theta_1 d \cos \theta_1} = -\frac{2}{3} . \quad (12)$$

$$\langle \cos \theta_2 \rangle = \frac{\int_0^1 \cos^2 \theta_2 d \cos \theta_2}{\int_0^1 \cos \theta_2 d \cos \theta_2} = \frac{2}{3} . \quad (13)$$

With

$$\frac{\Delta E}{E} = \frac{1 - \beta \cos \theta_1 + \beta \cos \theta_2 - \beta^2 \cos \theta_1 \cos \theta_2}{1 - \beta^2} - 1 . \quad (14)$$

So the energy gain is given by:

$$\frac{\Delta E}{E} = \epsilon \simeq \frac{4}{3} \beta . \quad (15)$$

This is the energy gained every time the particle passes the shock front. Since the magnetic field around this shock front is turbulent, the particle will cross the shock front many times gaining energy every time. After crossing the front  $n$  times, the energy is given by:

$$E_n = E_0(1 + \epsilon)^n . \quad (16)$$

So in order to reach a certain energy  $E$  the particle needs to cross the shock front  $n$  times:

$$n = \ln \left( \frac{E}{E_0} \right) / \ln(1 + \epsilon) . \quad (17)$$

But there is also a probability  $P_i$  (proportional to  $V$ ) that the particle will escape from the medium. The probability  $P_{E_n}$  that the particle escapes with an energy greater or equal to  $E_n$  is given by:

$$P_{E_n} = P_i \sum_{j=n}^{\infty} (1 - P_j)^n = (1 - P_i)^n . \quad (18)$$

We can fill in  $n$  here to obtain:

$$P_{E_n} = (1 - P_i)^{\ln\left(\frac{E}{E_0}\right)/\ln(1+\epsilon)} . \quad (19)$$

$$\ln P_{E_n} = \frac{\ln\left(\frac{E}{E_0}\right)}{\ln(1+\epsilon)} \ln(1 - P_i) . \quad (20)$$

$$\ln P_{E_n} = \frac{\ln(1 - P_i)}{\ln(1 + \epsilon)} \ln\left(\frac{E}{E_0}\right) . \quad (21)$$

So we get:

$$\frac{N}{N_0} = P_{E_n} = \left(\frac{E}{E_0}\right)^{-\alpha} . \quad (22)$$

$$\frac{dN}{dE} \propto \left(\frac{E}{E_0}\right)^{-\gamma} . \quad (23)$$

with

$$\alpha = -\frac{\ln(1 - P_i)}{\ln(1 + \epsilon)} \cong \frac{P_i}{\epsilon} . \quad (24)$$

and

$$\gamma = \alpha + 1 . \quad (25)$$

So we see that the first-order Fermi acceleration mechanism predicts an energy spectrum with a power law with an almost constant index ( $P_i$  and  $\epsilon$  are both proportional to  $\langle\beta\rangle$ ). In case of a supersonic shock  $\alpha$  is predicted to be around 1 ( $\gamma \sim 2$ ). First-order Fermi acceleration is currently considered as the mechanism responsible for accelerating high-energy cosmic rays [5].

## 3.2 Sources of Cosmic Rays

A handful of astrophysical objects are identified as potential sources of cosmic rays with high energies. These sources have been plotted in figure 3. In the figure we see the maximum energies up to which particles could be accelerated by the given sources. This is estimated by  $E_{max} \sim \beta_s z B L$ . Where  $\beta$  is the shock velocity in terms of the speed of light,  $z$  is the absolute value of the charge,  $B$  is the magnetic field and  $L$  is the size of the accelerator. In this chapter we will explore some of these objects as well as the acceleration mechanism of the cosmic rays.

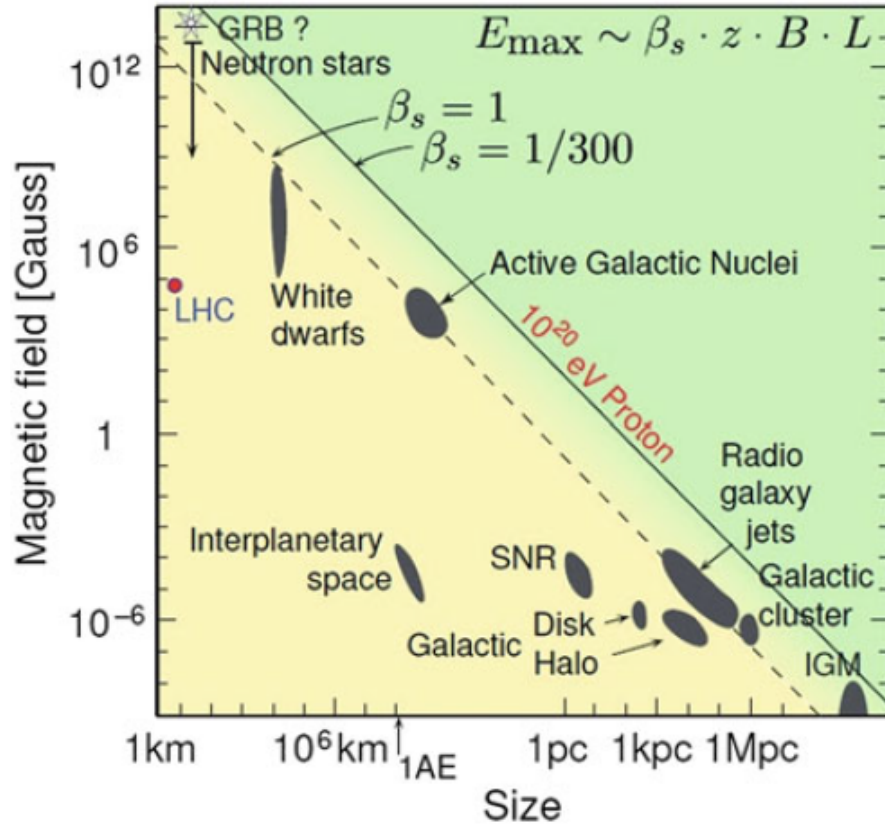


Figure 3: Hillas plot. Diagonal lines in this figure correspond to particular values of maximum energy [5]

### 3.2.1 Supernova Remnants

When a heavy mass star ( $\sim 8 M_{\odot}$  or greater) reaches the end of its lifetime it can no longer use nuclear fusion to generate thermal pressure to support against the gravitational pressure [6] [7]. Since the outward pressure can no longer support the star, it will collapse. When this happens, rapid neutron capture causes elements to form which are even heavier than iron (this is where all elements heavier than iron come from). The collapse is followed by a violent explosion, called a supernova. What is left in the center is a black hole or neutron star (depending on the mass of the star). In this process most of the mass of the star is blown away. The material which is blown away from the core is called a supernova remnant (SNR).

Two specific supernova remnants have been observed with the Fermi Large Area Telescope (LAT) from 2008 to 2012 [8]. These SNRs (IC 443 and W44) were observed since they are surrounded by molecular clouds and therefore are the most luminous SNRs. The ages of the remnants are estimated to be around  $\sim 10,000$  years. And they are located at a distance of 1.5 kpc (IC 443) and 2.9 kpc (W44). The gamma rays from the decaying pions around the SNRs could be measured with the Fermi LAT. This happens through the following reaction:  $p + p \rightarrow \pi^0 + \text{other products}$  followed by  $\pi^0 \rightarrow 2\gamma$ . The energy of these photons is  $m_{\pi^0}c^2/2 = 67.5$  MeV in the pion rest frame. In order to show that these gamma rays belong to pion decay and not to bremsstrahlung of electrons it is shown that these gamma rays follow the "pion decay bump". This is shown in figure 4, it is seen that the measurements clearly follow the  $\pi^0$  decay model. Lastly, in the same figure the energies of the cosmic

rays as inferred from the observed gamma rays are plotted. It is concluded that the power law of the proton energies of both supernovae has an index of 2.3 – 2.4.

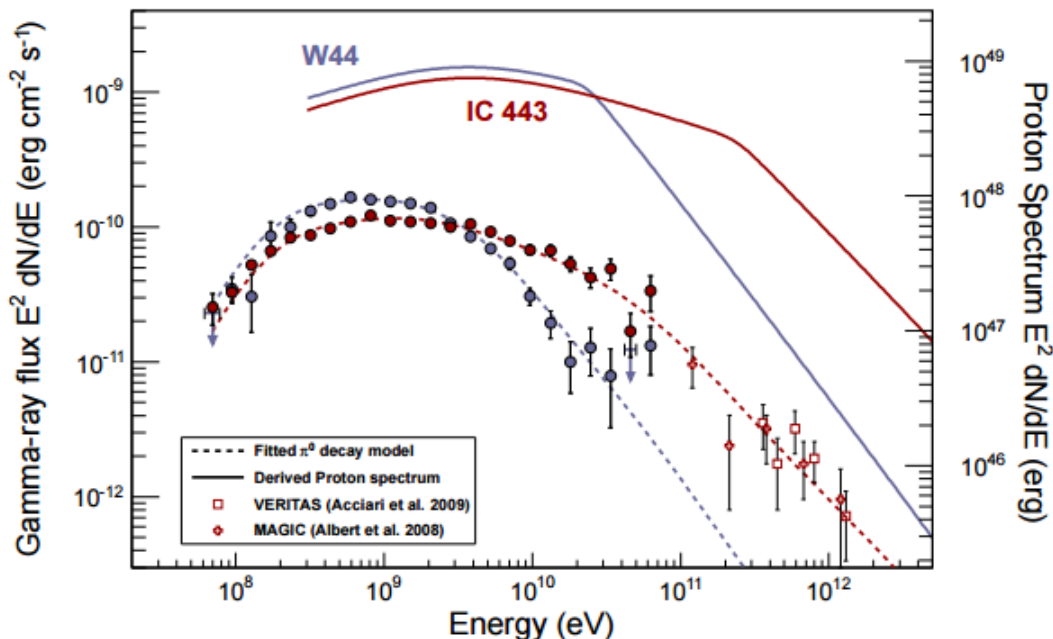


Figure 4: The gamma ray spectrum and derived proton spectrum for W44 and IC 443 [8]

### 3.2.2 Galactic Centre

With the High Energy Spectroscopic System (HESS) gamma rays from the galactic centre were observed for 10 years [9]. The studied region extends to a radius of 250 pc at positive galactic longitudes and 150 pc at negative galactic longitudes. These observed gamma rays also come from pion decay caused by cosmic rays. The spatial distribution of the cosmic ray density was plotted as a function of distance from Sagittarius A\* (Sgr A\*). From figure 5 it is concluded that this corresponds to a  $1/r$  radial profile. This dependence indicates a quasi-continuous injection of protons into the central zone. Furthermore, the energy spectrum of diffuse gamma rays was plotted and it was concluded that the best fit to the data is a power law with an index of  $\sim 2.3$  up to energies of tens of TeV. The energies of these gamma rays imply that the highest cosmic ray energies would be around 1 PeV. For the gamma ray spectrum from pion decay as observed by HESS it was concluded that the best fit is a power law with an index of  $\sim 2.4$ .

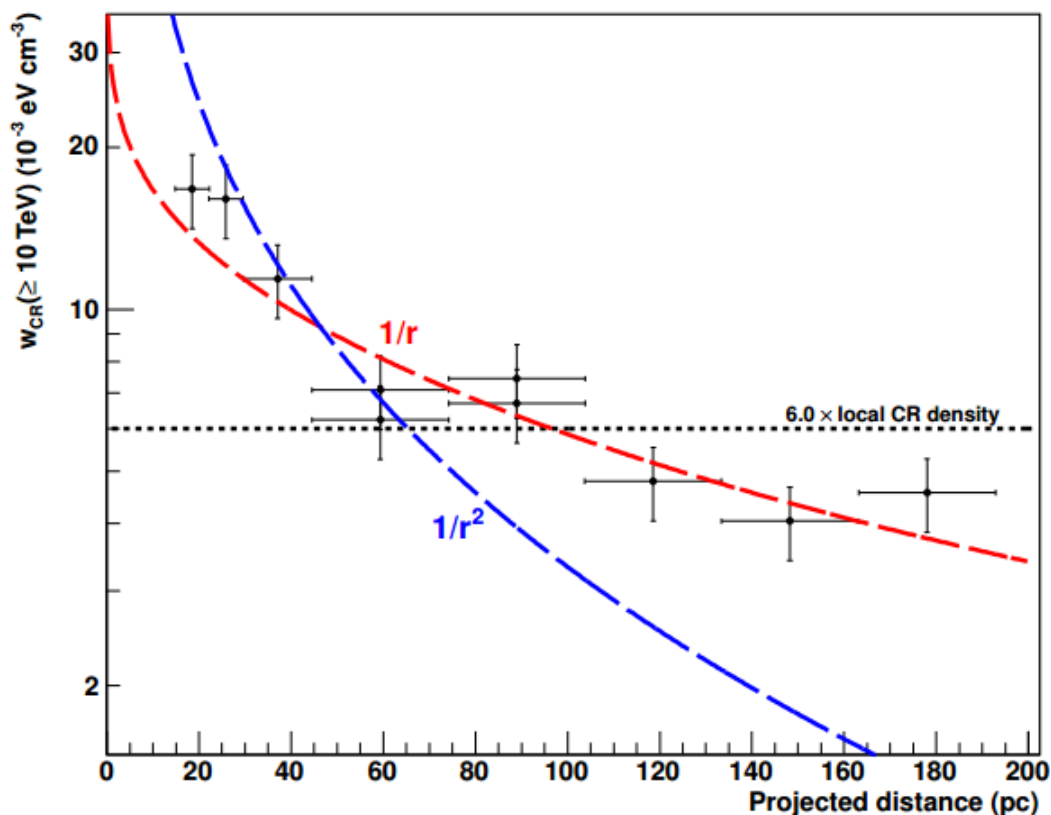


Figure 5: The cosmic ray density as a function of projected distance to Sgr A\*, it is clear that the HESS data supports a  $1/r$  profile [9]

If Sgr A\* is the source of the petaelectronvolt particles it is concluded that the acceleration rate (of about  $10^{37-38}$  erg/s) which is necessary for these protons is two or three orders of magnitude higher than the current bolometric luminosity of Sgr A\* [9]. Furthermore, these cosmic rays would use up about 1% of the power produced by accretion onto the black hole. At certain epochs the accretion rate could have been a lot higher than it is presently. This could also produce more cosmic rays than is does currently which would explain the observed gamma rays and inferred cosmic ray energies.

### 3.2.3 Active Galactic Nuclei

Almost all galaxies have a super massive black hole at their center [3]. These black holes accumulate mass through accretion. In about 10% of the galaxies this accretion disk and a jet (perpendicular to the galaxy) are observed to be so luminous that they outshine the entire galaxy. The galactic nuclei in which this phenomenon is observed are called Active Galactic Nuclei (AGN). Another property of AGN is that their luminosity is variable, furthermore they have a lot of non-thermal radiation emission in all wavelengths. From the jets that are formed in these AGN shock fronts can be produced. Therefore AGN are a good candidate for accelerating cosmic rays to very high energies.

In 2007 the Pierre Auger Collaboration published an article [10] about the correlation of the highest energy cosmic rays with nearby extragalactic objects (such as AGN). Given that most of the cosmic rays are protons, it is stated that only sources within 200 Mpc of the earth can produce cosmic rays with energies above  $6 \cdot 10^{19}$  eV. If these cosmic rays originate from sources further than 200 Mpc

they will interact with the CMB and lose energy (GZK limit). Using the Pierre Auger observatory it is shown that the observed cosmic rays with these energies are correlated to the positions of AGN. This correlation can be seen in figure 6.

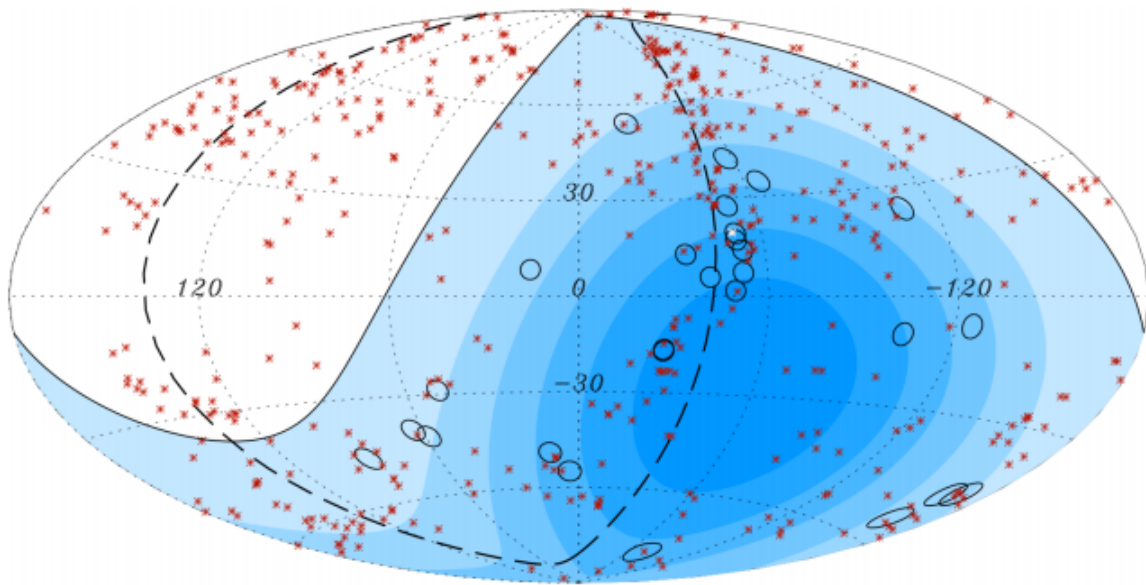


Figure 6: The correlation between the observed high energy cosmic rays and nearby AGN. The blue circles indicate the arrival direction of cosmic rays and the red asterisks are nearby AGN. Furthermore Centaurus A is indicated by a white asterisk. The darker area indicates a longer exposure time [10]

## 4 Lightning Mapping Array

Early lightning studies were conducted as an attempt to understand the stepped leader process. This was mostly done by Schonland between 1938 and 1956 [11]. The method which was used was by making photographs of a lightning discharge. Later streak photographs were made by Berger and Vogelsanger [2] in order to have an idea how stepped leaders evolve in time. Since the stepped leader process is very dynamic, photographs are not the most insightful method.

In recent years lightning mapping arrays have been constructed in order to study the lightning process. These arrays usually consist of simple antennas to measure radio waves emitted from stepped leaders. If we can measure the stepped leaders very accurately we can reconstruct the lightning strike from the cloud to the ground. First we will discuss the lightning mapping array in New Mexico. Then we will take a look at LOFAR and how it can be used as a lightning mapping array.

### 4.1 Accuracy of the Lightning Mapping Array in New Mexico

The accuracy of the New Mexico Lightning Mapping Array has been investigated experimentally and the data which is used for this analysis is obtained during the operation of STEPS [12] (Severe Thunderstorm Electrification and Precipitation Study) which was conducted in 2000. The New Mexico Lightning Mapping Array network has 13 stations spread over a  $60 \times 80$  km area. The arrival time of the signals were determined in  $80 \mu\text{s}$  time intervals. The events are measured when the peak of the signal exceeds a threshold value (which is adjustable). This threshold is calibrated in such a way that the threshold is exceeded about  $\simeq 100 - 1000$  times per second without lightning. This is caused by noise such as radio frequency interference (RFI). Furthermore, the stations can be operated in a high-rate mode which is used for detailed lightning studies. When the stations are in this mode the time intervals which are measured drop from  $80 \mu\text{s}$  to  $10 \mu\text{s}$ . At each station there is a GPS receiver present which outputs a pulse every second which is accurate to a few tens of nanoseconds rms. One of the timing errors is caused by the fact that arrival times are quantized in 40 ns increments which gives a rms error of  $\frac{40}{\sqrt{12}} \simeq 12$  ns.

The accuracy of the measurements was determined by locating a sounding balloon which carried a GPS receiver and a very high frequency transmitter. From the sounding balloon pulses of 63 MHz in frequency and 125 ns in duration were transmitted. From the differences in measurements between the GPS receiver and the LMA observing the pulses from the very high frequency transmitter a timing uncertainty could be determined.

The New Mexico Lightning Mapping Array uses a time of arrival (TOA) technique in order to determine the location and time of the measured sources from lightning. This is done using the following equation:

$$c(t - t_i) = \sqrt{(x - x_i)^2 + (y - y_i)^2 + (z - z_i)^2} . \quad (26)$$

Given at least four measurements of  $t_i$ ,  $(x, y, z, t)$  can be determined. For the error analysis, only events which were measured from at least six different stations were taken into account, even though only four measurements are necessary. This is done to check the validity of the measurement. The timing uncertainty turned out to be a bit higher if fewer stations measured the event. For ten stations the best fit of the uncertainty turned out to be  $\Delta t = 43$  ns, for six stations this best fit turned out to be  $\Delta t = 48$  ns. This means that if there is a source over the network between 6 and 12km that

the location is measured accurate to 6-12m rms horizontally and 20-30 rms vertically.

This error analysis has also been done for actual lightning data. A difference is that the sounding balloon emitted well-defined pulses but lightning does not, therefore the uncertainty increases. The result of this analysis is that the rms error for lightning is about 50 ns (46 ns for ten stations, 53 ns for six stations) [12].

## 4.2 LOFAR as a Lightning Mapping Array

The LOw-Frequency ARray, or LOFAR, consists of 50 stations spread over Europe [13]. Most of the stations are located in the Netherlands with dense cluster core called the superterp. Every station consists of 96 low band antennas and 48 high band antenna tiles, except the international stations, they have 96 high band antenna tiles. The frequency range of the antennas is 30 – 80 MHz (low band) and 120 – 240 MHz (high band). Furthermore the antennas measure two polarization directions. LOFAR was built to perform astronomical measurements in the radio regime below 250 MHz. LOFAR is the first radio telescope which uses simple omni-directional antennas as compared to the usual antennas. All the signals from the different stations can be combined in order to form the signal of a conventional antenna.



Figure 7: The LOFAR superterp. ©Top-Foto, Assen

LOFAR has opened up a new region for radio observations and a couple of key science projects have been linked to LOFAR, namely: Epoch of Reionisation, Deep extragalactic surveys, Transient

sources, Ultra high energy cosmic rays, Solar science and space weather, Cosmic magnetism. None of these key science projects are directly related to lightning research, although high energy cosmic rays do play a role in lightning inception. The fact that lightning research can be done with LOFAR is something that was not thought of beforehand. It turns out that stepped leaders emit radio waves at frequencies we can measure with the low band antennas.

What makes LOFAR unique compared to the lightning array in Mexico is that LOFAR has a very high temporal resolution ( $\sim 1$  ns). Since stepped leaders are about  $1 \mu\text{s}$  in duration, this temporal resolution should let us explore the stepped leader process in much more detail. Furthermore, if we would use the time of arrival method with LOFAR just as it was done in Mexico, we should be able to locate the source of the received pulses to submeter accuracy. Since lightning research is not one of LOFAR's key science projects there are still ways to improve LOFAR to gain more data for lightning research. As of now lightning data is obtained manually by a LOFAR researcher. For the future it would be desirable if we could build a trigger at for example the LOFAR superterp. This trigger could go off whenever a lightning flash is observed in the optical regime, if at this point the transient buffer boards would send their data to save we should have data from the stepped leaders which produced this flash.

LOFAR	New Mexico Lightning Mapping Array
Able to read out full time spectrum	Arrival time of signals in $10 \mu\text{s}$ intervals
Accuracy of $\sim 1$ ns	Arrival time quantized in 40 ns increments
Observing range of 30-80 MHz	Observing range of 60-66 MHz
Measures two polarization states	Measures one polarization state
50 stations in Europe with 48 low band antennas each	13 measurement stations with 1 antenna each

Table 1: Comparison between LOFAR and the New Mexico Lightning Mapping Array [12] [13]

## 5 Lightning Observations

### 5.1 Lightning observations with LOFAR

The main goal of this research project is to determine the time and location at which a pulse from a stepped leader was emitted. One of the ways to do this is through the time of arrival method. With this method we look for time differences of the pulse arrival time between different stations. Since the diameter of the superterp is about 300 m. We know that the time difference can be at most 1  $\mu$ s. If we can determine the time differences we can use the following equation to find the location and time at which the pulse was emitted.

$$c(t - t_i) = \sqrt{(x - x_i)^2 + (y - y_i)^2 + (z - z_i)^2} . \quad (27)$$

Lightning measurements have been done twice with LOFAR in 2013. The first data set is from the 19<sup>th</sup> of june 2013, the second data set is from the 24<sup>th</sup> of july 2013. For my research I mostly worked with the first data set. These measurements were done with some central stations (including some of the superterp) and some remote stations, but no international stations.

In 2015 a python program was developed by Roxana Dina and Jeroen Muller [14] [15] in order to process the data observed by LOFAR . For our analysis we used their program and we made some adaptations to it.

### 5.2 Data analysis

#### 5.2.1 Time trace measurement

In figure 8 we see the time trace for a single antenna in CS002. We can clearly see some peaks from radio emission. In order to use the time of arrival method we need to compare the time traces for every antenna in every station.

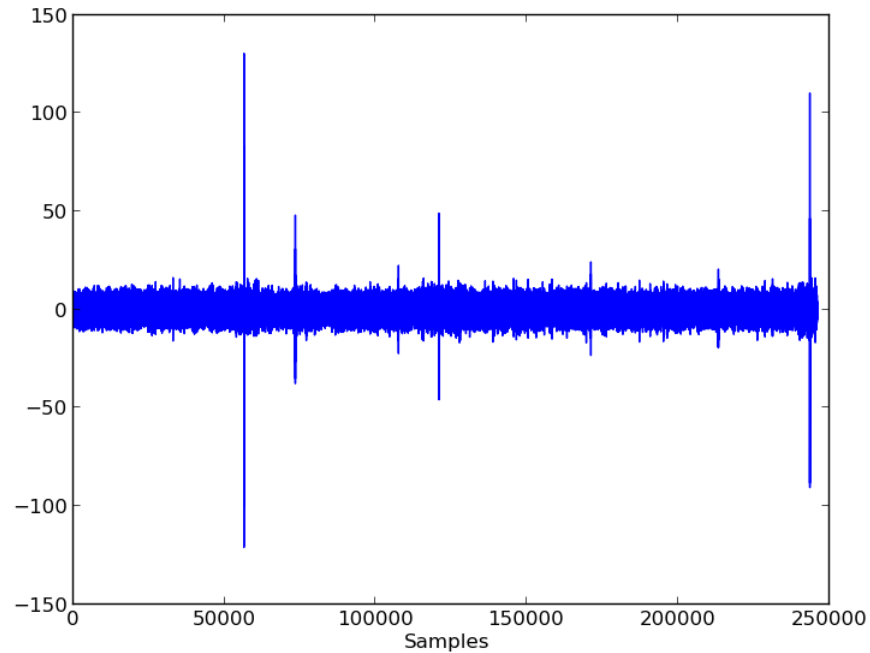


Figure 8: The received pulse is plotted as a function of time. The samples are 5 ns each, so this total time trace is around 1.25 ms

### 5.2.2 Time synchronization

First we will plot the time traces as we receive them as a function of time for the stations we used. This is done in figure 9. The size of the circles indicates the strength of the pulse. From this figure we see that the time differences between different stations is in the order of microseconds. Since this is too large to be a time difference due to a difference in arrival time of the pulse, this is a timing issue of LOFAR itself. This is clear for example if we compare the received pulses at CS004 and CS006, both of these stations are situated on the LOFAR superterp. Since the diameter of the superterp is around 300 meter we know that the time difference in the signal is at most  $1 \mu\text{s}$ . In figure 9 we see that the time difference is of the order of  $100 \mu\text{s}$ .

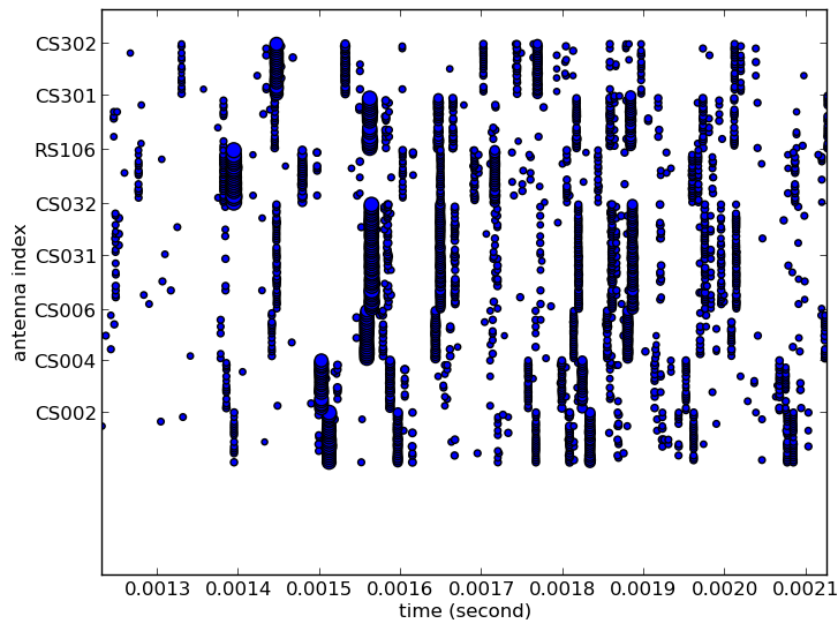


Figure 9: A plot of the pulses as received by a number of LOFAR stations. On the vertical axis we have the different stations so this has no physical meaning. CS stands for Central Station and RS stands for Remote Station. We can see that there are microsecond differences between the same pulses in different stations. This indicates that the LOFAR stations do not have the same absolute time.

Since the timing differences are too large we cannot calculate the position or the time of the origin of the emission this way. However, we can set a pulse as a reference and remove the offsets for the other stations. This way the reference pulse should line up in every station. In order to do this first we find the strongest pulse in every station, since the strongest pulse should be the same pulse in every station. We apply all these offsets and plot it again in figure 10 in order to check if it worked.

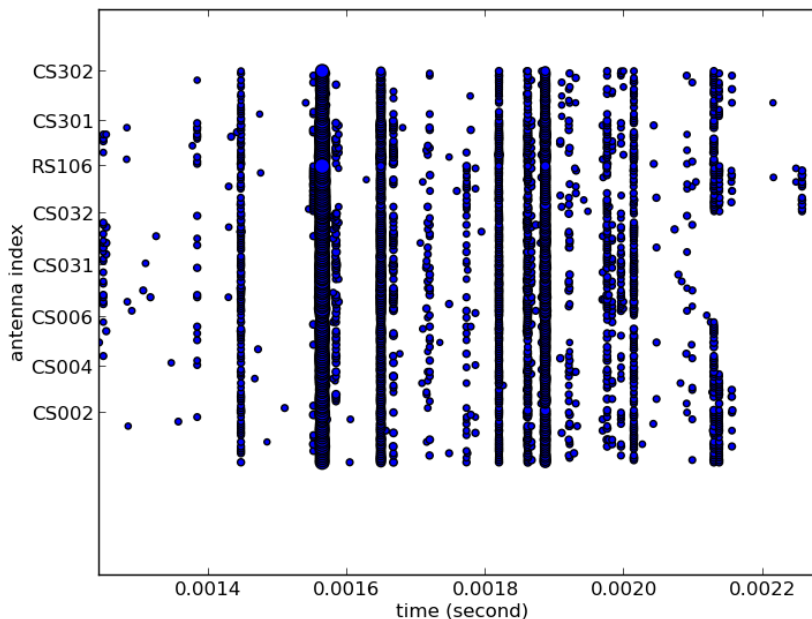


Figure 10: A plot of the same pulses as in 9 after removing the offsets. We see that the strongest pulse lines up very well (just before 0.0016 seconds). We also see that a lot of other pulses line up very well.

### 5.2.3 Pulse shape

We will zoom in on the strongest pulse as measured in the time frame of the curtain plot. From inspection we see that this strongest pulse is emitted between 1.5 and 1.6 microseconds. For stepped leaders we expect a sharp peak since the stepped leader is basically a charge which accelerates or decelerates for a short period of time [2].

We will examine the pulse shape for one polarization state for every central station around the strongest pulse. The length (in time) of the trace we will inspect are 200 samples of 5 ns each, so a total length of 1  $\mu$ s. Every pulse here is the average of the pulses of all the antennas within that station. We will plot the Hilbert envelope of the received signal. This is an envelope over the sinusoidal signal we receive. This will also get rid of the negative amplitudes. In figure 11 we see that the pulse shapes overlap very well. This tells us that the pulse really belongs to the same stepped leader. Furthermore besides the large peak we also observe a second peak right behind it. Since this pulse is consistent in every station we know that this is something physical and not just noise.

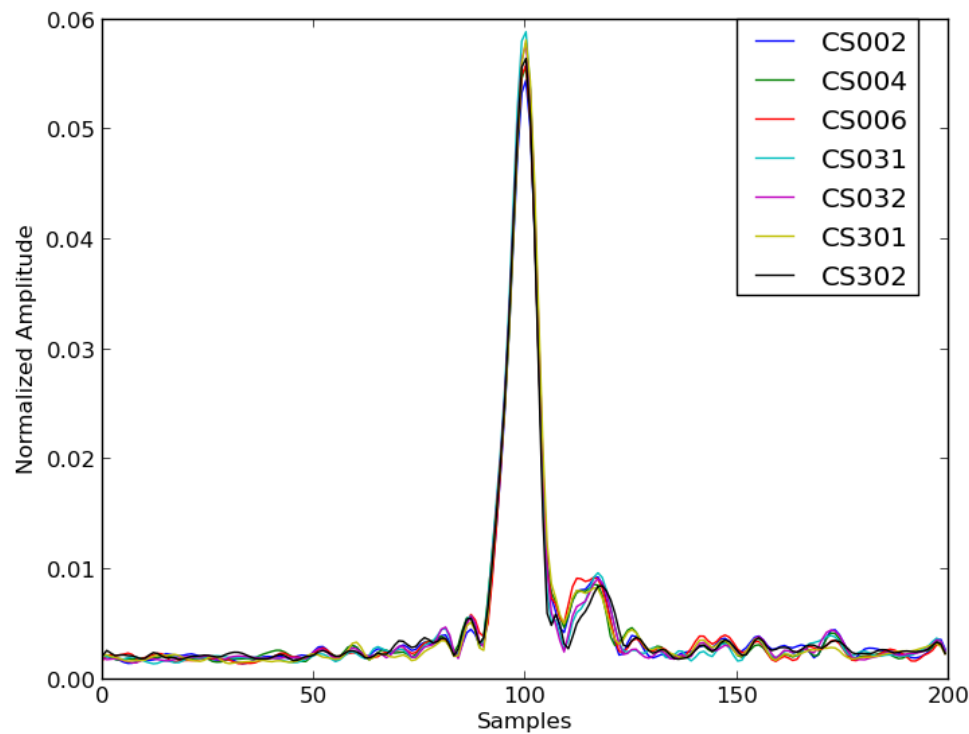


Figure 11: The pulse shape plotted for the central stations we used, the average is taken over all antennas within each station for one polarization direction

#### 5.2.4 Time of arrival method

To further investigate into this second pulse we will compare the pulse shapes between two different stations, a central station (CS002) and a remote station (RS106). The pulse shapes are plotted in figure 12 and 13. In these plots we have the average pulse as observed in every antenna of CS002 and RS106. In the pulse shape of the central station we can still clearly see the secondary pulse right behind the main peak. However in the remote station it seems that this secondary pulse arrives earlier at the station as compared to the central station. This is an indication for the second pulse originating from a different point in space and/or time.

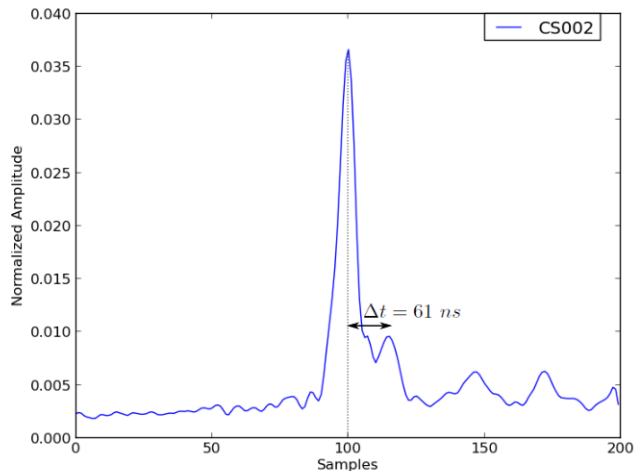


Figure 12: The pulse shape as observed in CS002

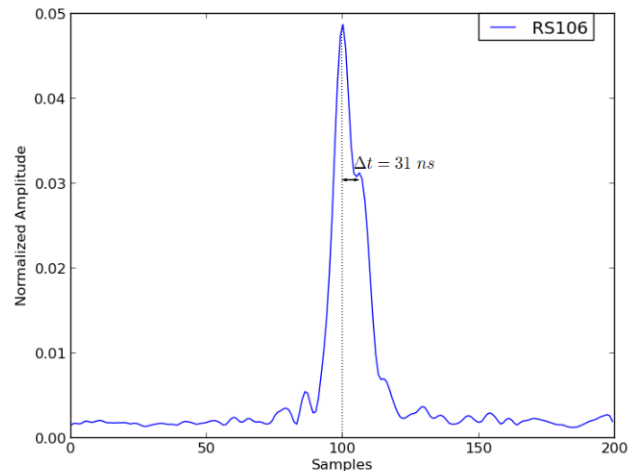


Figure 13: The pulse shape as observed in RS106

Furthermore, the time difference is given in figure 12 and 13. From this time difference we can try to use the time of arrival method for the secondary pulse. Since we are only using two time differences we have to make some assumptions. We assume that the secondary pulse is parallel to the line between CS002 and RS106 and we assume that the secondary pulse is emitted later in time than the first pulse. With these assumptions and the measurements now we will calculate the spatial separation between the first and second pulse. In figure 14 we see a sketch of our situation. We know  $r_0$ , the distance from CS002 to RS106 so we know  $\theta$ . From the geometry of the situation we can calculate  $r_2$  and  $r_3$ .

$$r_2 = \sqrt{(r_0 + 3.4)^2 + 8.3^2} . \quad (28)$$

$$r_3 = \sqrt{(r_0 + 3.4 - x \sin \theta)^2 + (8.3 - x \cos \theta)^2} . \quad (29)$$

$$c(61 - 31) \cdot 10^{-9} = r_2 - r_3 . \quad (30)$$

Where  $r_0$ ,  $r_2$ ,  $r_3$  can be seen in figure 14 and  $c$  is the speed of light. Now we can calculate  $x$ , and this turns out to be 24.2 m. This result really highlights the accuracy of LOFAR.

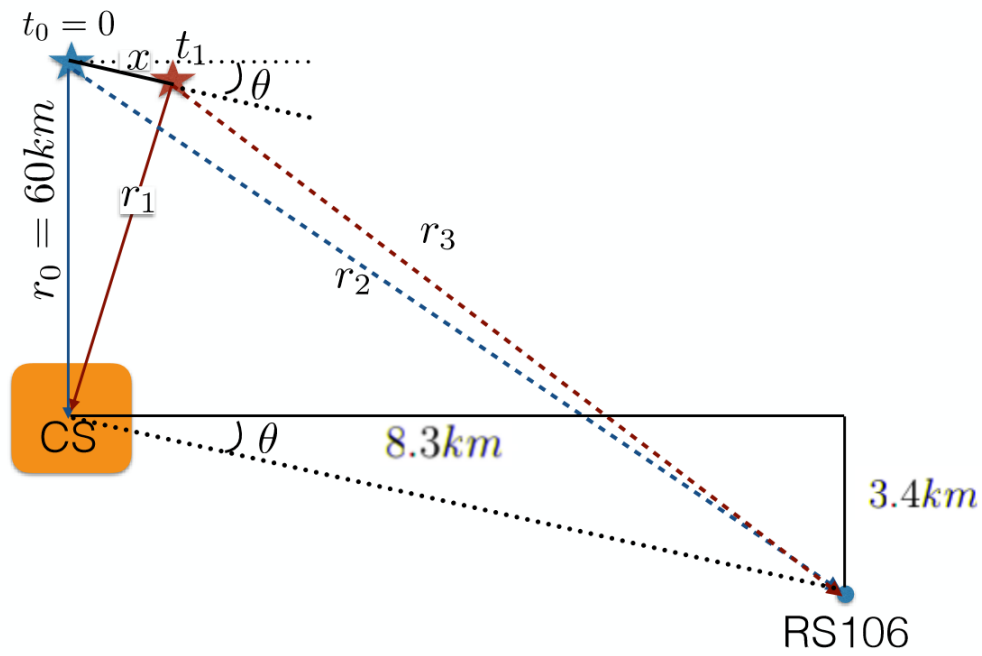


Figure 14: A sketch of the time of arrival method as used for the secondary pulses we observe in CS002 and RS106, we know that the lightning event happens around 60 km north of CS002 through data from the weather observatory (KNMI)

## 6 Conclusion and Outlook

In order to investigate the lightning process we first looked at lightning inception and it turns out that in a thundercloud we need an electric field, hydrometeors and enough free electrons. In air there are not enough free electrons to start this process so they have to come from another source. This source turns out to be extensive air showers caused by cosmic rays. We have seen that these cosmic rays originate from sources such as supernova remnants, the galactic centre and active galactic nuclei. Then stepped leaders will form a conducting channel between the cloud and the ground. It turns out that, since these stepped leaders are charges which accelerate and decelerate, they emit radiation. This radiation can be observed by LOFAR in the low band antennas. One of the big steps to use LOFAR as a lightning mapping array is the time synchronization of the pulses between different stations. We have succeeded in doing this by taking the strongest pulse in every station in a given time frame and taking one station as a reference. Furthermore we have looked at the pulse shape of the strongest pulse in the the same time frame as the curtain plots. With two assumption we could perform the time of arrival method for this secondary pulse and it turns out that the secondary pulse is 24.2 m away from the first pulse. This result really highlights the accuracy of LOFAR and is really promising for future research.

At the moment the time differences are too large between stations so it is not feasible to use the time of arrival method between stations. If this timing issue could be resolved in the future we should be able to use the time of arrival method between stations. However there is another way to use the time of arrival method, in stead of comparing arrival time differences at different stations we could compare the arrival time of the pulse in different antennas within a single station. This is possible since all antennas within a station have the same timing. We can do this for multiple stations and determine the origin of the pulse. If we are able to determine the origin of the pulse accurately we can follow the lightning discharge from the cloud to the ground and learn about the characteristics of stepped leaders.

## References

- [1] Anna Dubinova, Casper Rutjes, Ute Ebert, Stijn Buitink, Olaf Scholten, and Gia Thi Ngoc Trinh. Prediction of lightning inception by large ice particles and extensive air showers. *Phys. Rev. Lett.*, 115:015002, Jun 2015.
- [2] A. Vladimir Rakov and A. Martin Uman. *Lightning: Physics and Effects*. Cambridge University Press, 2003.
- [3] Gijsbert Tijsseling. Modeling a dual mirror cherenkovtelescope to analyse pointing precision. Master's thesis, VU University Amsterdam, 9 2014.
- [4] ENRICO Fermi. On the origin of the cosmic radiation. *Phys. Rev.*, 75:1169–1174, Apr 1949.
- [5] Alessandro de Angelis and Mrio Joo Martins Pimenta. *Introduction to Particle and Astroparticle Physics: Questions to the Universe*. Springer-Verlag, 2015.
- [6] Marc L. Kutner. *Astronomy: A physical perspective*. Cambridge University Press, 2003.
- [7] B. Burke and F. Graham-Smith. *An Introductcion to Radio Astronomy*. Cambridge University Press, 2010.
- [8] M. Ackermann et al. Detection of the Characteristic Pion-Decay Signature in Supernova Remnants. *Science*, 339:807–811, February 2013.
- [9] HESS Collaboration, A. Abramowski, F. Aharonian, F. A. Benkhali, A. G. Akhperjanian, E. O. Angüner, M. Backes, A. Balzer, Y. Becherini, J. B. Tjus, and et al. Acceleration of petaelectronvolt protons in the Galactic Centre. *Nature*, 531:476–479, March 2016.
- [10] J. Abraham et al. Correlation of the highest energy cosmic rays with nearby extragalactic objects. *Science*, 318:939–943, 2007.
- [11] B.F.J. Schonland. The Lightning Discharge. *Encyclopaedia of Physics*, 22.
- [12] Ronald J. Thomas, Paul R. Krehbiel, William Rison, Steven J. Hunyady, William P. Winn, Timothy Hamlin, and Jeremiah Harlin. Accuracy of the lightning mapping array. *Journal of Geophysical Research: Atmospheres*, 109(D14), 2004. D14207.
- [13] LOFAR. Homepage of lofar, 2016.
- [14] Jeroen Muller et al. Lightning induced by collision of cosmic particles hitting earths atmosphere., 2015.
- [15] Roxana Dina. Analysis of lightning radio emmissionsn, 2014.

## 7 Appendix

Running instructions for Lightning scripts from Jeroen (based on those of Roxana Dina)

1.

Make sure you have the following programs in your directory:

```
bottleneck
lightning.py
index.py
imp.py
units.py (if you use Qader's version)
lofarsoft
```

1.2

Run script "index.py" with 2 arguments:

1st argument is the directory with the H5 files

2nd argument is the file name that is created (use index.txt)

This creates a numpy array that contains file names that will be processed in following step

```
$ python index.py /somedirectory index.txt
```

2.

Start python shell:

```
$ ipython
```

2.1

```
>> import lightning as l
```

this loads all lightning scripts and loads the index file created in step 1 as 'l.i' (only v

2.2

This step is just for clarity, not actually necessary!!

```
>> for b in l.get_blocks():
```

```
>>     l.clean_block(b)
```

This cleans the data and changes b.cleaned to True

2.3

Also not strictly necessary, just for clarity!!

```
>> for b in l.get_blocks():
```

```
>>     l.find_pulses(b)
```

If b.cleaned is not set to True this step will also do the cleaning

## 2.4

This step will do everything at once, find the pulses and clean as well

```
>> p = l.find_pulses_iterate(l.get_blocks())  
with default arguments this loads 'index=l.i'  
this also performs RFI cleaning etc.
```

Optional:

You can save the pulse array in a file using:

```
>> np.savefig('pulsefile_name', p)
```

Then you can load these as:

```
>> p = np.load('pulsefile_name.npy')
```

## 2.5

In this step we will plot the data

```
>> l.curtain(p)
```

To get a curtain plot we go from index --> blocks --> pulse array --> curtain plot

If you ssh into another machine (APP):

WINDOWS: you need an extra program in order to get this working graphically (Xming or MobaX)

LINUX: No problems (don't forget to use -X to get it working graphically)

## 2.6

Here I explain how to get the offsets between the stations and remove the offsets in order to have the stations lined up on the curtain plot

first we have to calculate the offsets:

```
>> offsets = l.calculate_offsets(p)
```

as far as, I have perceived from the lightning script, this module calculates the offsets between the largest pulses

to apply the offsets in order to line up the station:

```
>> p_apply_offsets = l.apply_offsets(p, offsets)
```

A more decent way is to avoid altering the timing between the antennas in the same station. to do this, we need to update offsets as follows:

```
>> offsets = l.offsets_reduce_station(offsets)  
>> p_apply_offsets = l.apply_offsets(p, offsets)
```

Optional operations:

A handy shortcut is to use:

```
>> p = l.pulses(optional arguments)
```

This will do `get_blocks` and `find_pulses_iterate` in one step.

To get the pulses from a single (or multiple) antenna(s) you can use:

```
>> p = l.pulses(stations=['XXXXX', 'XXXXX'])
```

So we can use for example CS002, and then we can also do a curtain plot via

```
>> l.curtain(p)
```

To take a different time block for the data to be evaluated you can use:

```
>> p = l.pulses(start_time = [l.t[x]])
```

default is `t[4]` and `t` has 9 elements

To make a 2d plot of the stations which are used for the measurements (the stations are taken

```
>> l.plot_stations()
```

To create a normalized envelope for all pulses in each station (one pulse per station) and p

```
>> p = l.find_pulses_iterate(l.get_blocks())
```

```
>> l.compare_envelope_stations(p)
```

```
#####
```

I reproduced Jeroen's plot by using the following commands:

```
>> p = l.pulses(stations=['CS302', 'CS301', 'RS106', 'CS032', 'CS031', 'CS006', 'CS004', 'CS002'])
```

```
>> offsets = l.calculate_offsets(p)
```

```
>> offsets = l.offsets_reduce_station(offsets)
```

```
>> p_apply_offsets = l.apply_offsets(p, offsets)
```

```
>> l.curtain(p_apply_offsets)
```

These timeblocks correspond to the same timeframe and stations Jeroen used.

Here is the steps to get the plot of the correlated waveforms:

```
In [2]: import lightning as l
```

```
In [3]: import numpy as np
```

```
In [4]: pulses = np.load('pulses_b30-30.npy')
```

```
In [5]: l.curtain(pulses)
```

```
In [6]: p_apply_offsets = l.apply_offsets_auto(pulses)
```

```
In [7]: l.curtain(p_apply_offsets)
```

```
In [9]: event = l.get_pulses_interval(p_apply_offsets, t1 = 1.51, t2 = 1.52)
```

```
In [11]: selected_pulses = l.get_correlated_pulses(event, plot = True, correlation_coefficient = 0.5)
```

```
In [12]: selected_pulses = l.get_correlated_pulses(event, plot = True, correlation_coefficient = 0.5)
```

To make `combine_envelope_cc099.png`:

```
In [xx]: selected_pulses = l.get_correlated_pulses(event, plot = True, correlation_coefficient = 0.5)
```

In `apply_offsets_auto` you can change polarization

To get timeseries of one antenna:

```
timeseries = l.get_simtimeseries_data(start_time = 0.0012288, samples = 245760)
plt.plot(timeseries[3])
plt.show
```

# Lightning stepped leaders; LOFAR data and simulations

The initial and yet fundamental process in a typical cloud-to-ground lightning strike includes the propagation of a very faint and charged channel which is called stepped leader. The exact mechanism for the step leaders is not understood. The reason for this is that the temporal and/or spatial resolution of the devices exploited for observing this phenomenon has not been sufficient. The radio interferometric array of LOFAR however is capable to measure radio signals with 1 ns temporal resolution. Thus LOFAR can measure the radio pulses emitted by stepped leaders at multiple times during the formation of the steps and locate the positions of the pulses with sub-meter accuracy. This provides with new possibilities to test and probe the theories explaining the propagation of a stepped leader. We are currently processing the data measured by LOFAR, and in addition, are preparing a simulation tool to calculate the radio signals expected on the basis of current models. By comparing the simulation and experimental data, we aim to determine the characteristics of stepped leader formation.

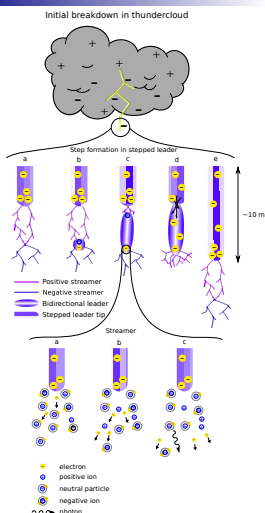


# Lightning stepped leaders; LOFAR data and simulations

## Stepped leader theory

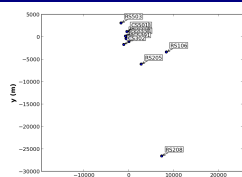
Stepped leaders make the first conducting path that connects the thundercloud to the ground in a negative cloud-to-ground discharge. It starts from an initial discharge in the cloud.

- Streamers form at the leader tip. The air gets heated and becomes more conductive. A space stem might appear at the branching of a streamer.
- When the space stem gets hot enough, it can transform into a bidirectional leader. It is now more ionized, more conductive and more luminous.
- The leader tip and the bidirectional leader grow towards each other.
- A new step is formed when they connect. Charge flows in, and a corona burst follows.
- The process repeats.

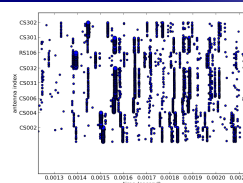


- The very high electric field at the tip accelerates free electrons.
- accelerated electrons collide with air molecules and ionize some of them. This results in more free electrons that are accelerated: an electron avalanche forms.
- Electrons may instead be captured by air molecules, excite air molecules or recombine with positive ions. Photons produced by relaxation or recombination might ionize air molecules elsewhere.

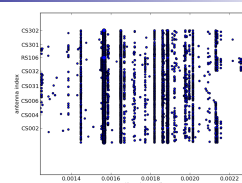
## LOFAR Measurements



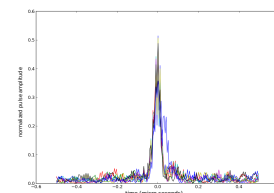
In the top left plot we see that LOFAR stations that were used for lightning measurements. The stations in the middle are core stations, while the outer stations are remote stations. For our measurements we used the low-band antennas.



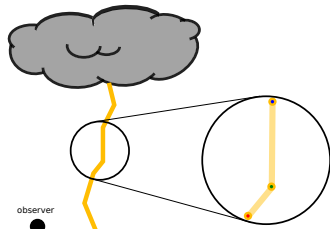
In the left curtain plot we see the data as measured and see that the pulses we receive arrive at different stations at different times. In the right curtain plot we synchronized the time of the pulses between different stations. Since we are able to synchronize the times we are able to use a time of arrival method in order to determine the time and location of the emitted pulses. As of now this has not yet been done and still is a work in progress.



Here we see the pulse shape of a single pulse (the strongest pulse) as measured by LOFAR. The same stations are used here as in the curtain plot. For a stepped leader we expect a sharp peak with little structure besides this. In the plot we see some structure and since this is consistent in almost every station we know that this is intrinsic to the signal and not just noise. At the moment it is unclear why there is this structure in the pulse shape and what this means.

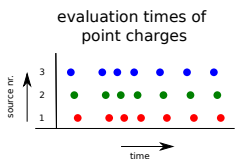


## Simulation

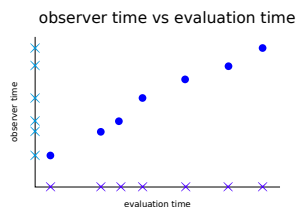


A series of connected straight line currents is used to model the stepped leader.

Using the principle of superposition and a numerical integration scheme, the line currents are approximated by a set of point charges.

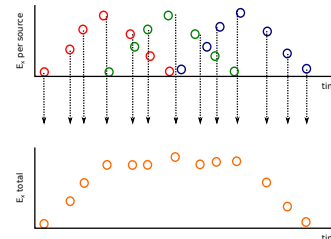


Choose for each point charge a suitable time grid to evaluate the electric field it produces. Take small time steps in intervals where the produced electric field changes rapidly



The electric fields travel at the speed of light. Therefore the observer receives them at some later time, depending on the distance the fields have to travel. When the point charge is moving, this means that the time grid spacing changes.

## electric fields at observer



For each point charge, calculate the electric field and the corresponding arrival time at the observer

Combine the observation time grids of the individual point charges into a new time grid. Then interpolate the electric fields of the point charges to obtain the fields at the new time points. Add these fields to obtain the total electric field on the new time grid.

# Goal of the project

# LOFAR as a Lightning Mapping Array

Danny Sardjan

Rijksuniversiteit Groningen  
KVI - Center for Advanced Radiation Technology  
Kapteyn Institute

July 18, 2016

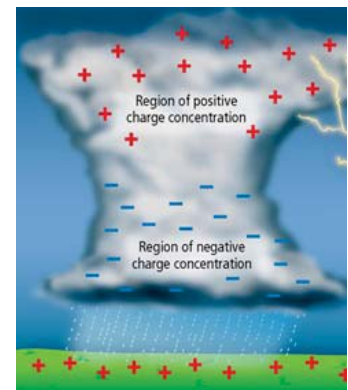
- Use LOFAR to determine the origin of stepped leaders in space and time through their emission of radio signals

# Outline

- Lightning Inception
- Cosmic Rays
- Lightning Propagation
- LOFAR as a Lightning Mapping Array
- LOFAR Measurements

# Lightning Inception

- Thunderstorm Electric Field
- Hydrometeors
- Free Electrons (Extensive Air Showers)



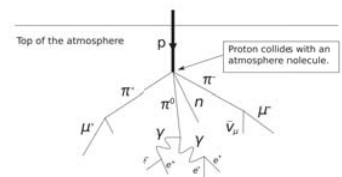
# Lightning Inception

- Thunderstorm Electric Field
- Hydrometeors
- Free Electrons ( $100 \text{ cm}^{-3}$ )



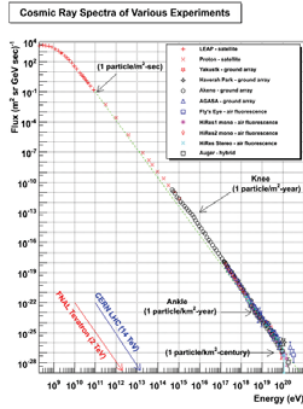
# Extensive Air Shower

- Source of free electrons: Extensive Air Showers caused by Cosmic Rays
- Link between Lightning and Astronomy



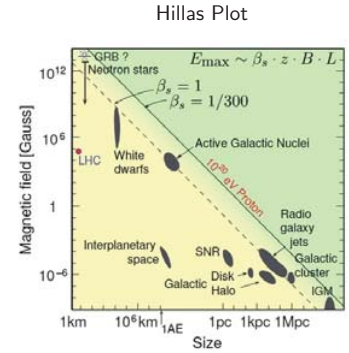
## Cosmic Rays

- Cosmic Ray Spectrum
- Follows a power law of  $\sim E^{-2.7}$



## Cosmic Ray Sources

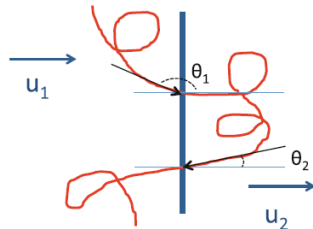
- Potential sources of Cosmic Rays
- Cosmic Rays with energies of  $\sim 10^{15}$  eV are of interest for lightning inception



de Angelis and Martins Pimenta (2015)

## Fermi Acceleration

- $\frac{\Delta E}{E} \approx \frac{4}{3}\beta$ .
- $\frac{dN}{dE} \propto \left(\frac{E}{E_1}\right)^{-\gamma}$
- $\gamma$  expected to be around 2 for a shock

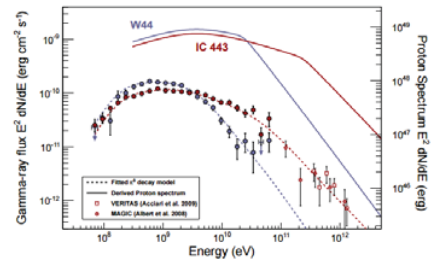


de Angelis and Martins Pimenta (2015)

## Cosmic Ray Sources

- Observations with Fermi LAT
- Pion Decay

### Supernova Remnants



Ackermann et al. (2013)

## Lightning Propagation

- Stepped Leaders
- 1  $\mu$ s in duration, 20 to 50  $\mu$ s interval
- Bridge distances of 10 to 50 meters

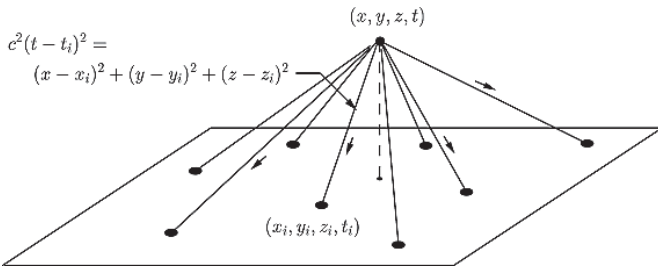


## Lightning Discharge

- Return Stroke
- Flash
- Neutralizes conducting channel

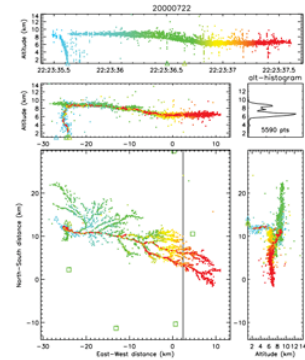


Time of Arrival method



Thomas et al. (2004)

New Mexico Lightning Mapping Array



Thomas et al. (2004)

Why LOFAR as a LMA?

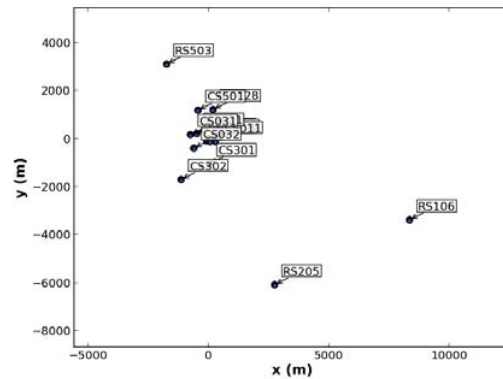
LOFAR Measurements

LOFAR

- Able to read out full time spectrum
- Accuracy of  $\sim 1$  ns
- Observing range of 30-80 MHz
- Measures two polarization states
- 50 stations in Europe with 48 low-band antennas each

New Mexico Lightning Mapping Array

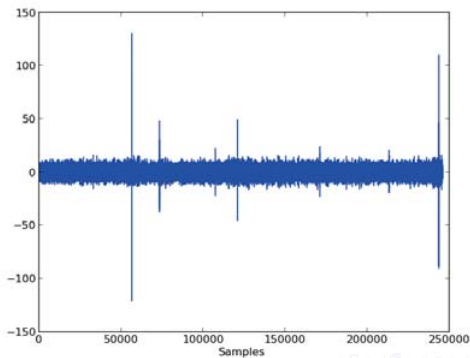
- Arrival time of signals in  $10 \mu s$  intervals
- Arrival time quantized in 40 ns increments
- Observing range of 60-66 MHz
- Measures one polarization state
- 13 Measurement Stations with 1 antenna each



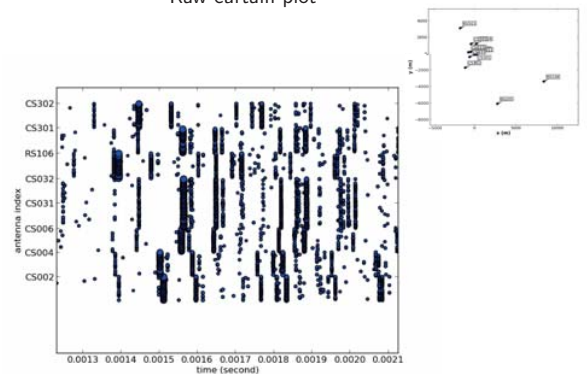
LOFAR Measurements

LOFAR Measurements

Time trace for a single antenna (CS002)

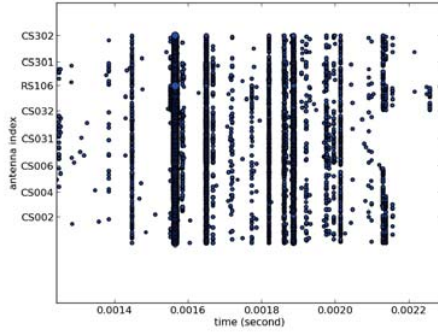


Raw curtain plot



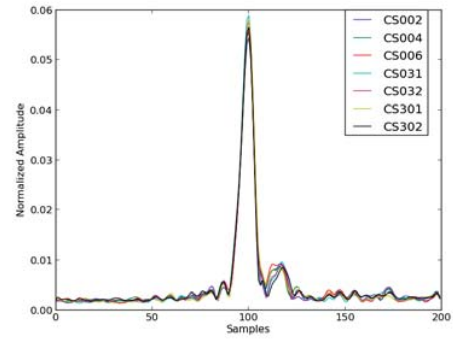
## LOFAR Measurements

Curtain plot after correction



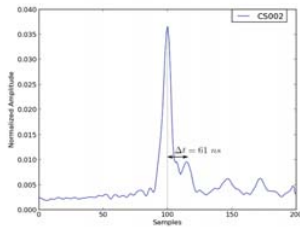
## LOFAR Measurements

Pulse shape (Hilbert envelope)

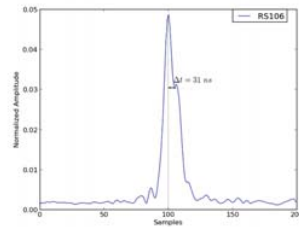


## LOFAR Measurements

Pulse shape CS002

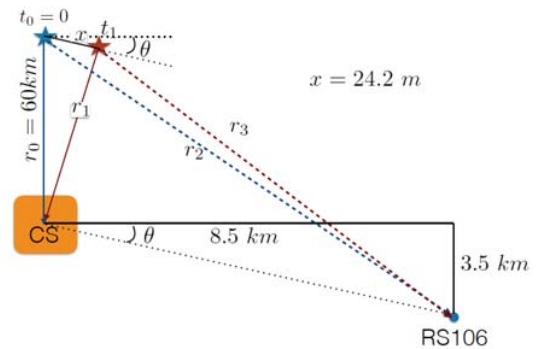


Pulse shape RS106



## LOFAR Measurements

Time of Arrival method



## Conclusion

- Removing the offsets yields the same pulse pattern in every station
- The distance between two pulses has been calculated very accurately using two pulse shapes

## Outlook

- Use Time of Arrival method within a station to determine location and time of emission
- Analyze new data from LOFAR